Enhanced Detection Using Target Polarization Signatures in Through-the-Wall Radar Imaging

Christian Debes, *Member, IEEE*, Abdelhak M. Zoubir, *Fellow, IEEE*, and Moeness G. Amin, *Fellow, IEEE*

***Abstract*—We consider the problem of through-the-wall radar imaging (TWRI), in which polarimetric imaging is used for automatic target detection. Two generalized statistical detectors are proposed which perform joint detection and fusion of a set of multipolarization radar images. The first detector is an extension of a previously proposed iterative target detector for multiview TWRI. This extension allows the detector to automatically adapt to statistics that may vary, depending on target locations and electromagnetic-wave polarizations. The second detector is based on Bayes' test and is of interest when target pixel occupancies are known from, e.g., secondary data. Properties of the proposed detectors are delineated and demonstrated by real data measurements using wideband sum-and-delay beamforming, acquired in a semicontrolled lab environment. We examine the performance of the proposed detectors when imaging both metal objects and humans.**

***Index Terms*—Detection, polarimetric imaging, radar imaging, through-the-wall.**

I. Introduction

THROUGH-THE-WALL radar imaging (TWRI) is an evolving technology [1]–[3] using electromagnetic (EM)-wave propagation to visualize scenes hidden behind walls or other visually opaque materials. It has numerous applications, including firefighter and police missions as well as military operations. Much of the work in the area of TWRI has considered analyzing and interpreting 3-D TWRI images [4], [5]. This includes performing automatic target detection [6]–[8] and classification [9]–[12]. However, these approaches are based on using single-polarization antenna systems.

There are two main approaches that have been introduced for detection of targets behind walls and inside enclosed structures. The first approach is image based and aims at developing a robust target detection scheme that iteratively adapts to varying statistics of the target images [6]–[8]. The argument for using an iterative learning scheme stems from the fact that the target image statistics clearly depend on the target 3-D orientation and position and can also vary with the imaging system specifications, resolutions, and standoff distance. The main objective is to devise 2-D and 3-D target detectors for TWRI, which incorporate distribution of the target intensity in the image domain, as shown by backprojection imaging algorithms.

The second approach directly works on the data, in lieu of an image, and aims at designing waveforms for target detection that exploit *a priori* information about the properties and characteristics of the targets of interest [13]. For TWRI applications, it is recognized that, in addition to humans, there are only a finite number of objects that are of interest inside rooms and behind walls, for example, guns and rifles of different sizes and possible shapes. As such, the underlying indoor imaging application is ideally suited for considering waveform design based on target signature exploitation. The objective of this matched illumination approach is to devise optimal signature exploitation waveforms for through-the-wall target detection, including humans and weapons, using a multiantenna radar system in monostatic, bistatic, and multistatic configurations. Both deterministic and stochastic extended target models have been considered for this purpose. This approach faces challenges in dealing with multiple targets and securing *a priori* information about the target positions and orientations.

The purpose of this paper is to expand on the first approach which has broad applications, with little or no requirements for advanced knowledge of target characteristics. Our goal is to improve detection by utilizing polarization diversity and accounting for changing image intensity distributions as a function of transmitter–receiver co- and cross-polarizations.

Existing works in polarimetric imaging for TWRI applications include those in [14]–[16]. In [14], a radar-signature-based approach for detecting stationary and moving weapons is proposed. The authors consider polarization information for the specific case of detecting a rifle in TWRI images. It was shown that the cross- to copolarization return ratio can be used to successfully discriminate between a human with and without a weapon. In [15], a polarization contrast technique that provides improved TWRI images by adapting the imaging system to the observations is proposed. The authors consider polarization difference imaging that shows improved enhancement in terms of image quality. An adaptive technique is proposed that finds the optimal combination of polarization signal channels. The polarization information is used in [16] to eliminate ghost targets that appear in TWRI images due to multipath propagation. As such, the image quality is strongly improved which facilitates target detection. The authors make use of time-difference radar imaging and frequency weighting to suppress the wall sidelobes. A multiplicative combination

Manuscript received March 24, 2011; revised July 11, 2011; accepted August 20, 2011. Date of publication November 24, 2011; date of current version April 18, 2012. The work of M. G. Amin was supported by the Office of Naval Research under Grant N00014101055.

C. Debes is with the AGT Group (R&D) GmbH, 64295 Darmstadt, Germany (e-mail: cdebes@agtgermany.com).

A. M. Zoubir is with the Signal Processing Group, Institute of Telecommunications, Technische Universität Darmstadt, 64283 Darmstadt, Germany (e-mail: zoubir@spg.tu-darmstadt.de).

M. G. Amin is with the Radar Imaging Laboratory, Center for Advanced Communications, Villanova University, Villanova, PA 19085 USA (e-mail: moeness.amin@villanova.edu).

Color versions of one or more of the figures in this paper are available online at http://ieeexplore.ieee.org.

Digital Object Identifier 10.1109/TGRS.2011.2170077

technique of co- and cross-polarized time-difference images is then considered to reduce the effect of ghost targets.

The contribution of this paper is to provide a general image-domain-based framework for automatic target detection, utilizing multipolarization images for TWRI applications. The aim is to jointly detect and fuse a set of TWRI polarimetric images to a single binary representation while maintaining a preset false-alarm rate. We hereby deal with stationary objects where Doppler analysis [17] or change detection techniques are inapplicable. Furthermore, as opposed to [15] and [16], we consider the statistical target detection problem in TWRI where postprocessing techniques are applied to obtain a binary image representation, given a set of polarimetric TWRI images. We consider two different detection approaches that adapt to image statistics, which vary with space and polarization. The first detector is based on an iterative version of the Neyman–Pearson (NP) test [6], [7] initially proposed for multiviewing TWRI and is generalized to deal with multipolarization TWRI images. The second detector is an iterative version of Bayes' test, allowing adaptation to unknown and changing image statistics. While the first detector allows presetting a nominal false-alarm rate, the second has a direct relation to scene sparsity in TWRI [18]. In most urban sensing applications, there are typically a small number of objects in a mostly empty room. Given a sufficient high resolution, this property renders most image voxels as background, whereas only a few voxels contain target reflections. This knowledge can be used by Bayes' test to set the probability of target occurrence.

This paper provides detection results using a calibrated experimental setup. It also considers the setup of a stationary human behind a wall. Since front walls obscure indoor targets, rendering target detection very difficult or impossible, we apply, for both setups, background subtraction, which makes use of empty or reference scene measurements. This approach removes, or strongly mitigates, the front wall returns, producing a high image quality. We also apply frequency weighting which considerably reduces wall effects by windowing in the frequency domain. The frequency weighting data processing can be applied with or without background subtraction. We note that, in this paper, we deal with postprocessing of radar images obtained through walls. A detailed description of the wideband sum-and-delay beamforming algorithms used in this paper can be found in [5].

This paper is structured as follows. In Section II, the two adaptive target detectors for TWRI are presented. An experimental setup using calibration objects and the corresponding detection results are shown in Section III. In Section IV, we consider the specific problem of detecting a stationary human behind a wall. Finally, Section V provides conclusions.

II. Target Detection in Polarimetric TWRI

Let $y_r(i,j,h)$ with $i=0,\ldots,N_i-1$, $j=0,\ldots,N_j-1$, $h=0,\ldots,N_h-1$, and $r=1,\ldots,R$ denote the set of acquired 3-D TWRI images using different polarizations. Here, i, j, and h are the coordinates in range, cross-range, and height, respectively, and N_i, N_j, and N_h are the numbers of voxels in range, cross-range, and height, respectively. The index r denotes the rth polarization with R being the number of polarizations used in the imaging system [19].

Given the set of R TWRI images, the aim of target detection is to provide a binary image $B(i,j,h)$ with $i=0,\ldots,N_i-1$, $j=0,\ldots,N_j-1$, and $h=0,\ldots,N_h-1$, which indicates the presence or absence of targets, i.e.,

$$B(i,j,h)=\begin{cases}1, & \text{target present at } (i,j,h)\\ 0, & \text{target absent at } (i,j,h).\end{cases} \tag{1}$$

In the following, we consider two different detectors based on the likelihood ratio that can be applied to image-domain-based target detection in TWRI. The first detector, presented in Section II-A, is an extension of our previous work [6], [7] to polarimetric TWRI. We demonstrate, how TWRI images obtained using multiple polarization can jointly be fused and detected by an iterative scheme. By using the new proposed scheme, the individual images are not assumed to be identically distributed anymore as in [6] and [7]. The second detector in Section II-B is a new iterative detector for TWRI that is based on Bayes' test [20]. We demonstrate how to fuse and binarize a set of polarimetric TWRI images while adapting to changing and unknown image statistics. Again, the individual images are not assumed to be identically distributed anymore. By using the proposed iterative Bayes' test, a direct connection to scene sparsity in TWRI is made.

A. Iterative NP Test

In [6] and [7], an iterative version of the Neyman–Pearon test was proposed for multiviewing TWRI, where a set of radar images is obtained using different vantage points. The iterative detector is applied in the image domain and allows one to adapt to changing image statistics by iteratively estimating the target and noise statistics. We propose to use the same framework for polarimetric TWRI by considering a pixelwise NP test as

$$\prod_{r=1}^{R}\frac{p_r\left(y_r(i,j,h)|H_1\right)}{p_r\left(y_r(i,j,h)|H_0\right)}\underset{H_0}{\overset{H_1}{\gtrless}}\gamma \tag{2}$$

where H_0 and H_1 denote, respectively, the null (target absent) and alternative (target present) hypotheses. The functions $p_r(\cdot|H_0)$ and $p_r(\cdot|H_1)$ are the conditional probability density functions (pdfs) under the respective hypotheses. The parameter γ is the likelihood ratio threshold, which can be obtained by fixing a desired probability of false alarm α as

$$\alpha=\int_{\gamma}^{\infty}p_L(L|H_0)dL \tag{3}$$

where $p_L(L|H_0)$ denotes the distribution of the likelihood ratio under the null hypothesis. Note that (2) implicitly assumes the target and noise realizations to be independent with respect to polarization r, but not necessarily identically distributed. This is of high practical importance, as the target statistics in the image domain generally vary when changing the polarization [21], [22].

By implementing the adaptive detector from [6] and [7], (2) is computed iteratively by jointly adjusting the pdf parameters

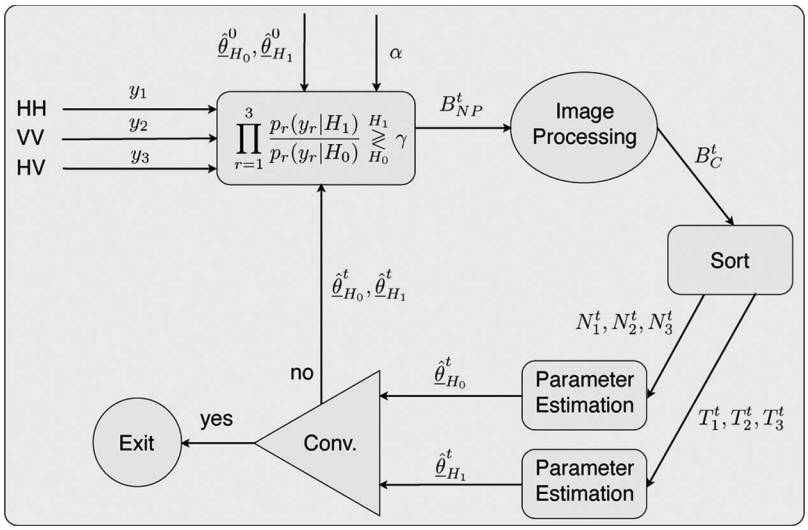

Fig. 1. Iterative detection scheme for polarimetric TWRI. The image statistics for HH, VV, and HV polarizations are estimated separately and then jointly fused by a likelihood ratio test.

to the image statistics at hand and optimizing the target and noise sets in the image domain using morphological filtering [23]. For polarimetric data, this scheme has to be generalized such that it can deal with polarization-dependent statistics. The generalized scheme is shown in Fig. 1, in which we consider the polarizations VV, HH, and HV, i.e., $R = 3$. Let the respective TWRI images obtained by VV, HH, and HV polarizations be denoted by y_1, y_2, and y_3, respectively. Furthermore, let $\underline{\hat{\theta}}^0_{H_0}$ and $\underline{\hat{\theta}}^0_{H_1}$ denote initial estimates of the parameter vectors $\underline{\theta}_{H_0}$ and $\underline{\theta}_{H_1}$ describing the pdfs under H_0 and H_1, respectively. Then, given a false-alarm rate α, a binary 3-D image B^1_{NP} can be obtained by evaluating (2), whereby the superscript 1 represents the first iteration. This image is generally prone to false alarms and missed detections. In the subsequent image processing step, an optimal morphological filtering step (see [12] for details) is employed to obtain the binary image B^1_C. This image can be used to provide the first description of the indoor scene and preliminary indication of targets and their locations. It can thus be used as a mask on the original polarimetric images to obtain target and noise sets $\mathcal{T}^1_r$ and $\mathcal{N}^1_r$ with $r = 1,\ 2,$ and 3, from which the revised parameter estimates $\underline{\hat{\theta}}^1_{H_0}$ and $\underline{\hat{\theta}}^1_{H_1}$ can be estimated. These revised parameter estimates are forwarded again to the NP test to obtain an improved detection result. The iteration stops when convergence is achieved, e.g., by observing a vanishing difference between subsequent parameter estimation.

The parametric pdfs $p_r(\cdot|H_0)$ and $p_r(\cdot|H_1)$ can be chosen based on an empirical image analysis study. As in [7], we invoke a Weibull noise and a Gaussian target pdf, which have been found to be valid models, also in polarimetric TWRI. Thus

$$\underline{\theta}_{H_0} = \begin{pmatrix} \kappa_1 \\ \kappa_2 \\ \kappa_3 \\ \lambda_1 \\ \lambda_2 \\ \lambda_3 \end{pmatrix} \quad \underline{\theta}_{H_1} = \begin{pmatrix} \mu_1 \\ \mu_2 \\ \mu_3 \\ \sigma_1^2 \\ \sigma_2^2 \\ \sigma_3^2 \end{pmatrix} \tag{4}$$

where κ_r and λ_r are the shape and scale parameters of the Weibull noise distributions and μ_r and σ_r^2 are the mean and variance of the Gaussian target distributions, with $r = 1, 2,$ and 3.

Note that, by considering the parameter setup from (4), as opposed to [6] and [8], the TWRI images using different polarizations are assumed to follow the same pdf model but differ in the respective parameters.

B. Iterative Bayes' Test

Making the same assumptions as in Section II-A, i.e., independence over polarization and assuming equal costs for correct decisions as well as equal costs for incorrect decisions, Bayes' test [20] can be written as

$$\prod_{r=1}^{R} \frac{p_r\left(y_r(i,j,h)|H_1\right)}{p_r\left(y_r(i,j,h)|H_0\right)} \underset{H_0}{\overset{H_1}{\gtrless}} \left(\frac{P_{H_1}}{P_{H_0}}\right)^R \tag{5}$$

where P_{H_1} and P_{H_0} are the probabilities of target and noise occurrence, respectively. It is noted that, in most radar applications, the NP test is preferred, as P_{H_1} and P_{H_0} are often unknown. In TWRI applications, however, one is often faced with imaging rooms that are mostly empty, and only few pixels in the corresponding radar image will be occupied by, e.g., human or furniture. This is more typical when performing background subtraction where most objects in the reference scene get eliminated. In this case, fixing P_{H_1} and P_{H_0} is more intuitive than fixing a false-alarm rate α, hence the consideration of Bayes' test.

When using Bayes' test as per (5), one faces the same problem as discussed in the previous section, i.e., the polarization-dependent statistics $p_r(y_r(i,j,h)|H_1)$ and $p_r(y_r(i,j,h)|H_0)$ are unknown and possibly space and time varying. We thus propose to iteratively estimate those unknown parameters similarly to the approach discussed in Section II-A. It is noted that the iterative framework, as shown in Fig. 1, can be considered by replacing the likelihood ratio threshold γ by $(P_{H_1}/P_{H_0})^3$. All

concepts, including the criteria of optimality and convergence as discussed in [12], remain unaltered.

III. Experimental Results: Calibration Scene

In this section, we review two techniques for wall removal and the corresponding changes for wideband sum-and-delay beamforming. Furthermore, the experimental setup is introduced, and detection results using a scenario with calibration metal targets are demonstrated.

A. Wall Removal

The wall does not only complicate the computation of the propagation delay between transceiver and target but also add strong distortions to the acquired radar image. Sidelobe effects from the wall may appear all over the radar image, thus overshadowing targets. As stated in the introduction, there are various effective methods for removing the wall clutter. Since this paper addresses the detection problem and not wall EM mitigations, we apply the method of background subtraction prior to detection. Background subtraction assumes empty, or reference, scene measurements being available, and it is considered the most effective wall removal technique. The empty scene signal returns are coherently subtracted from the signal returns of the populated scene. This practically eliminates primary wall effects and thus dramatically improves image quality. Secondary wall effects, e.g., interaction of targets with the wall, however, are not removed through this method. The use of background subtraction is ideal for long-term surveillance applications. In many practical applications, however, empty scene or reference scene measurements are not available.

A simple, yet effective, signal processing tool which can be used to improve image quality, with or without background subtraction, is frequency weighting. It is recognized that the image quality in TWRI, in the absence of wall subtraction, is mainly deteriorated due to the wall return sidelobe effects. The beamforming equation can be reformulated by using the concept of the system point spread function (PSF) as in [4] and [12]. The acquired image can then be written as the convolution of the target reflectivity and the PSF, i.e.,

$$I(u',v') = \Gamma(u',v') * *P(u',v') \tag{6}$$

where $**$ denotes the 2-D convolution and $P(u',v')$ is the PSF. The wall has a very strong reflectivity, and as such, the convolution operation performs a smearing in the image domain. This effect can be reduced by considering a frequency weighting, i.e.,

$$I_r^{\mathrm{FW}}(u',v') = \sum_{p=0}^{P-1}\sum_{l=0}^{L-1}\sum_{k=0}^{K-1} a_l \Gamma_r\left(u_p',v_p'\right) \times \exp\left(-j\omega_l\left(\tau_k(u',v') - \tau_k\left(u_p',v_p'\right)\right)\right) \tag{7}$$

where $\Gamma_r(u_p',v_p')$ is the complex target reflectivity when illuminating the pth target with the rth polarization [19], with $p = 0,\ldots,P-1$ and $r = 1,\ldots,R$. Furthermore, $\tau_k(u',v')$ is the two-way propagation delay when using the kth transceiver, and a_l is the lth frequency weight, $l = 0,\ldots,L-1$, with $\sum_{l=0}^{L-1} a_l = 1$. Classical frequency windows include Hamming, Hanning, and Blackman windows [24].

For illustration, Fig. 2 shows typical TWRI B-Scans (2-D cuts through the scene) of a metal dihedral obtained by wideband sum-and-delay beamforming. The images were obtained in a semicontrolled lab environment that will be detailed in the remainder of this section.

Fig. 2(a)–(c) shows the acquired images when performing the imaging without wall removal for VV, HH, and HV polarizations. The effect of convolving the target scene with the PSF is strongly visible and renders target detection practically impossible. As the wall has a weak cross-polarization signature, the convolution effect is strongly reduced when considering HV polarization as in Fig. 2(c). In Fig. 2(d)–(f), the imaging results based on background subtraction are shown. As can be seen, the coherent subtraction of empty scene measurements successfully removes the primary wall effects. The target can now clearly be seen in the upper left corner at approximately -2 ft cross-range and 15 ft down-range. It is noted that the dihedral is hardly visible in HV polarization as it has a weak cross-polarization signature. Finally, Fig. 2(g)–(i) shows the resulting B-Scans when using frequency windows as in (7). Here, we used a Hanning window for simplicity. It can be seen that frequency windowing sufficiently reduces the wall sidelobes and reveals the targets. However, as expected, the performance is noticeably worse compared to background subtraction. It is also noted that this technique loses its effectiveness for targets close to the wall.

B. Detection Results

In the following, the proposed detection schemes from Section II are evaluated for use in TWRI. We consider the setup shown in Fig. 3, which consists of a metal dihedral, trihedral, and sphere mounted on high foam columns. The targets are placed at approximately -2 ft cross-range and 14 ft down-range (dihedral), 0 ft cross-range and 9 ft down-range (sphere), and 4 ft cross-range and 12 ft down-range (trihedral). The scene is hidden behind a concrete wall with a thickness of 5.625 in and a dielectric constant of 7.66. A 57×57 element array is synthesized using a dual-polarization horn antenna with an interelement spacing of 0.875 in that is placed at a distance of 3 ft behind the wall. The scene is illuminated using a stepped-frequency signal with 801 frequencies uniformly spaced between 0.7 and 3.1 GHz. We consider VV, HH, and HV polarizations. Wideband sum-and-delay beamforming as in [5] is applied for image formation. We consider background subtraction as well as frequency weighting for wall removal.

For computational reasons, we consider the pixelwise log-likelihood ratio test $\Lambda(i,j,h)$ which, with $R = 3$, can be written as

$$\Lambda(i,j,h) = \sum_{r=1}^{3}\left[\ln\left(\frac{\lambda_r}{\sqrt{2\pi}\kappa_r\sigma_r}\right) - (\kappa_r - 1)\ln\left(\frac{y_r(i,j,h)}{\lambda_r}\right) + \left(\frac{y_r(i,j,h)}{\lambda_r}\right)^{\kappa_r} - \left(\frac{(y_r(i,j,h)-\mu_r)^2}{2\sigma_r^2}\right)\right]. \tag{8}$$

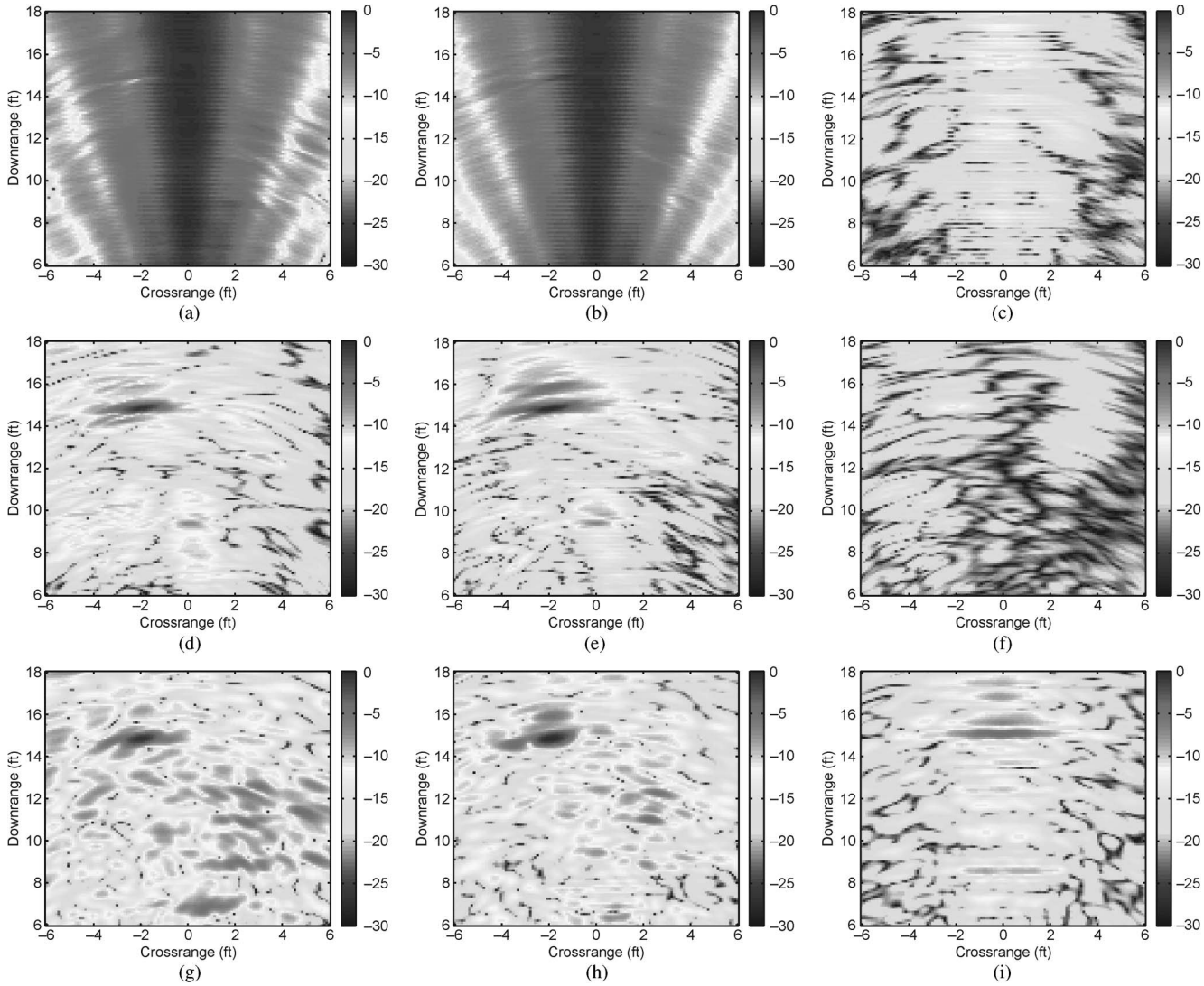

Fig. 2. Typical B-Scans using different wall removal techniques. (a) No wall removal, VV. (b) No wall removal, HH. (c) No wall removal, HV. (d) Background subtraction, VV. (e) Background subtraction, HH. (f) Background subtraction, HV. (g) Frequency weighting, VV. (h) Frequency weighting, HH. (i) Frequency weighting, HV.

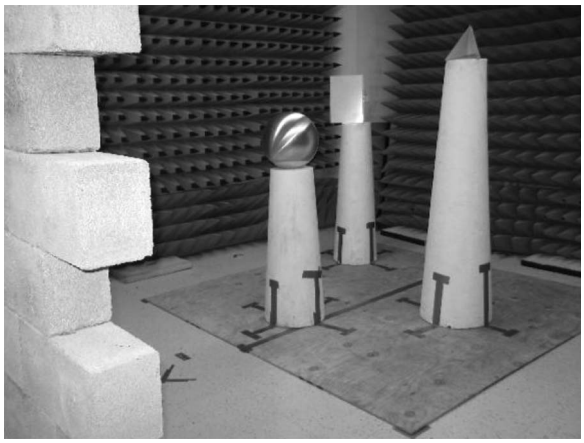

Fig. 3. Experimental setup: Calibration objects.

The parameters κ_r, λ_r, σ_r, and μ_r, where $r = 1$, 2, and 3, are estimated iteratively from the data as detailed in Section II using optimal morphological filtering [7], [8] to separate target and noise sets.

The detection results when using background subtraction for the single as well as full polarization are shown in Fig. 4. Here, the iterative NP test with a false-alarm rate of 5% is considered. It can be seen that the three targets of interest are visible in HH and VV polarizations [Fig. 4(a) and (b)] but are embedded in clutter. When using HV polarization in Fig. 4(c), the metal sphere (dashed ellipse) can no longer be detected, and there is increased clutter which complicates target detection. When performing fusion and detection of all three polarizations jointly, as per (8), improved detection is achieved, as evident in Fig. 4(d); clearly, all three targets are visible.

The detection results when using the iterative Bayes test introduced in Section II-B are shown in Fig. 5. Here, a ratio $P_{H_1}/P_{H_0} = 0.01$ is fixed. This corresponds to a target pixel occupancy of 1%. The ratio P_{H_1}/P_{H_0} directly relates to the knowledge of the sparsity of the 3-D scene. A ratio of 0.01 thus implicitly assumes that only 1% of all voxels are occupied by targets. This holds approximately true for the calibration scene considered here. The corresponding detection results

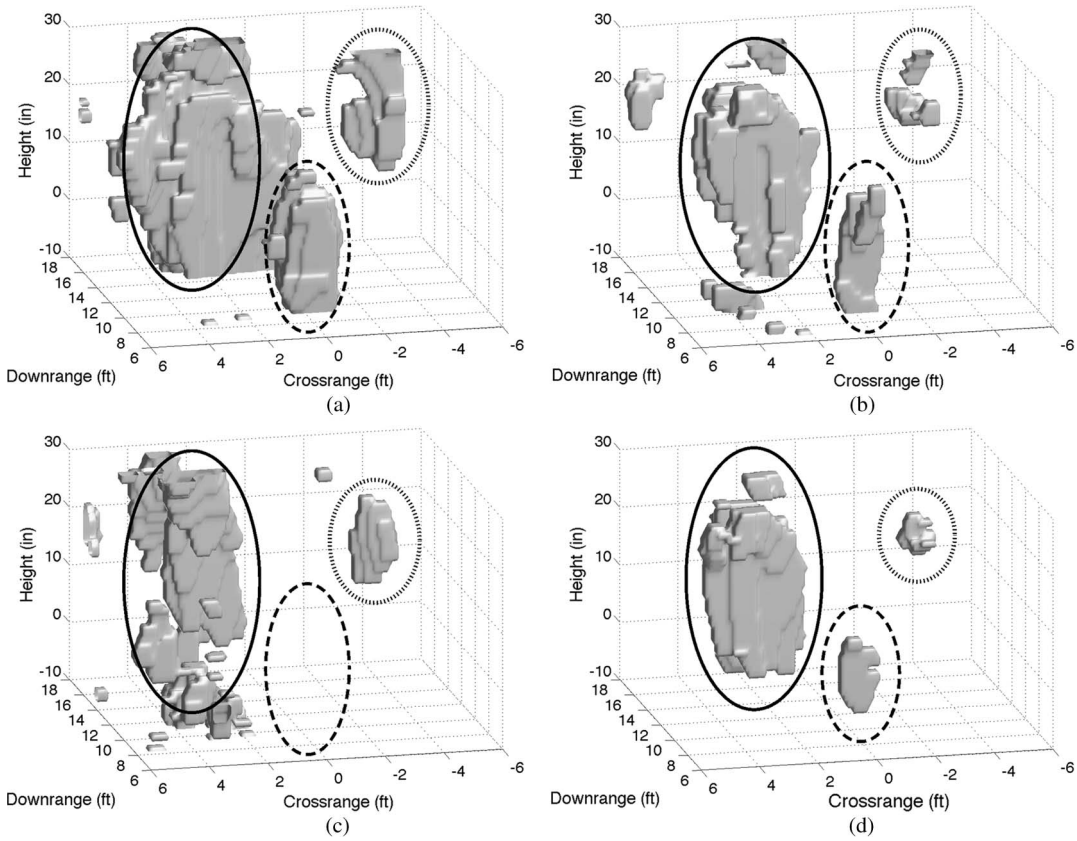

Fig. 4. Detection results of the iterative NP test of (solid) metal dihedral, (dotted) trihedral, and (dashed) sphere using single and full polarizations. Background subtraction is used for wall removal. (a) 3-D detection HH. (b) 3-D detection VV. (c) 3-D detection HV. (d) 3-D detection full polarization.

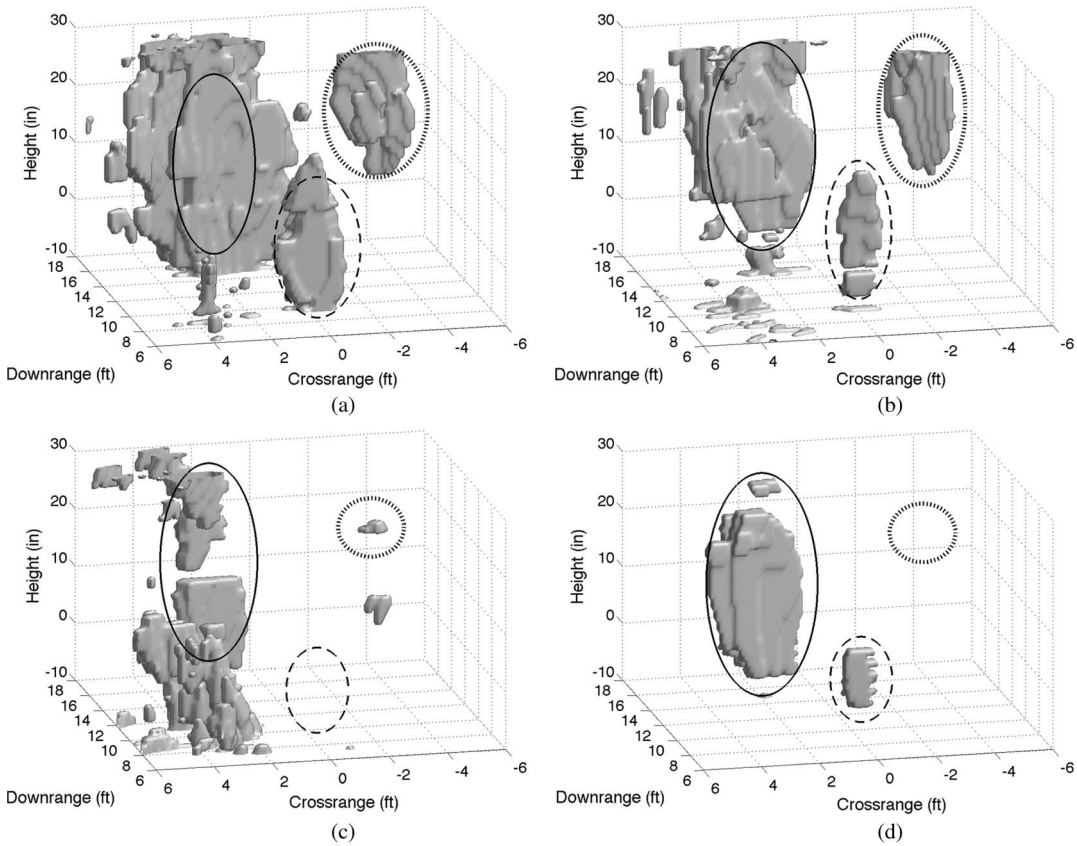

Fig. 5. Detection results of the iterative Bayes test of (solid) metal dihedral, (dotted) trihedral, and (dashed) sphere using single and full polarizations. Background subtraction is used for wall removal. (a) 3-D detection HH. (b) 3-D detection VV. (c) 3-D detection HV. (d) 3-D detection full polarization.

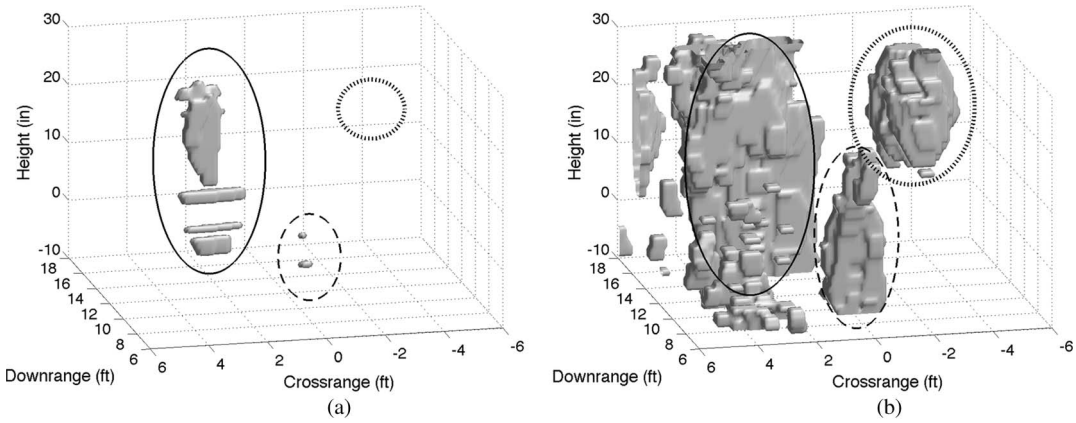

Fig. 6. Detection results of the iterative Bayes test of assuming target voxel occupancies of 0.1% and 10%. (a) $P_{H_1}/P_{H_0} = 0.001$. (b) $P_{H_1}/P_{H_0} = 0.1$.

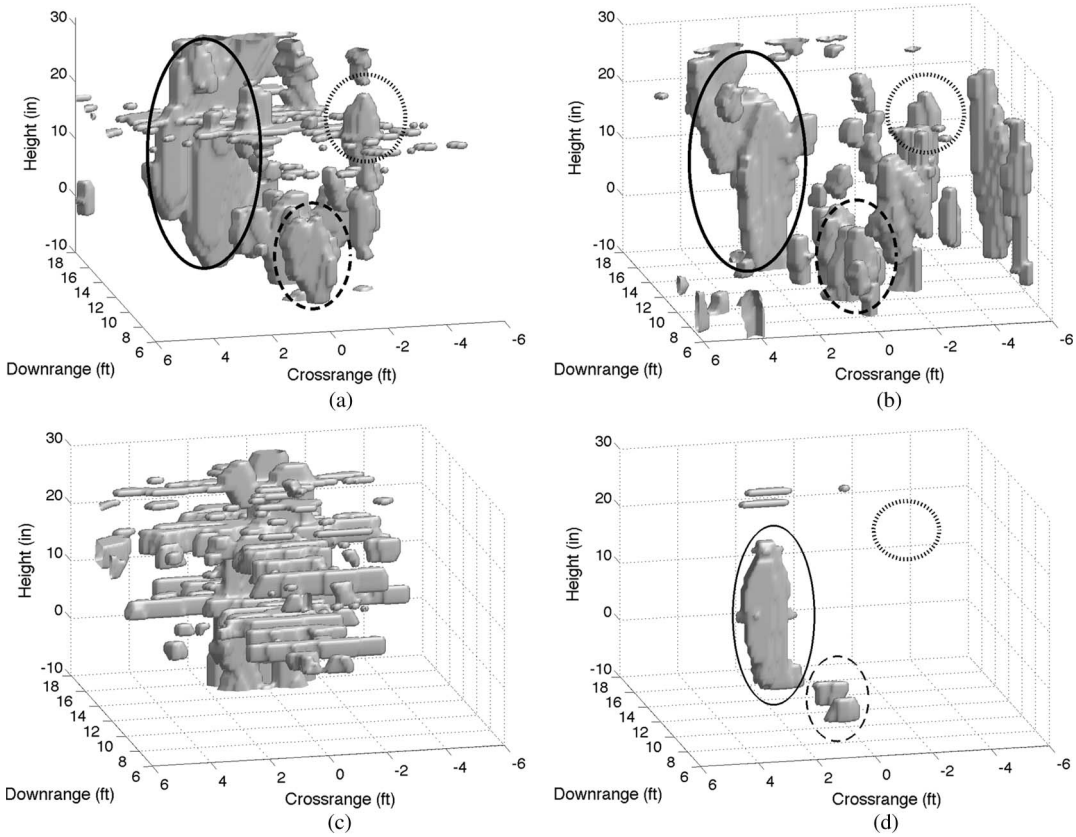

Fig. 7. Detection results of the iterative NP test of (solid) metal dihedral, (dotted) trihedral, and (dashed) sphere using single and full polarizations. Frequency weighting is used for wall removal. (a) 3-D detection HH. (b) 3-D detection VV. (c) 3-D detection HV. (d) 3-D detection full polarization.

when setting P_{H_1}/P_{H_0} to 0.001 or 0.1 are shown in Fig. 6. This corresponds to the implicit assumption of a target voxel occupancy of 0.1% or 10% which does not hold true for the scene considered. Given the detection result in Fig. 5(d), a similar result to the iterative NP test can be observed. The single-polarization images are affected by clutter, whereas the joint fusion and detection result enables detection of the dihedral and sphere. However, it is noted that, for this setting, the trihedral is not detected anymore. The reason for this stems from the fact that the trihedral has a rather small volumetric representation as it is "visible" only for few radar B-Scans. Furthermore, the cross-polarization signature, as shown in Fig. 5(c), is rather small, and as such, the morphological operations tend to suppress this object. By increasing the ratio P_{H_1}/P_{H_0}, the trihedral can be detected at the cost of an increase in clutter objects as shown in Fig. 6(b).

The detection results for the iterative NP test using a Hanning window for frequency weighting are shown in Fig. 7(a)–(c) for HH, VV, and HV polarizations. As already shown in the B-Scans in Fig. 2(g)–(i), the detectability of targets is decreased for the single polarized data. However, performing the proposed detection scheme, the three polarizations can be combined as

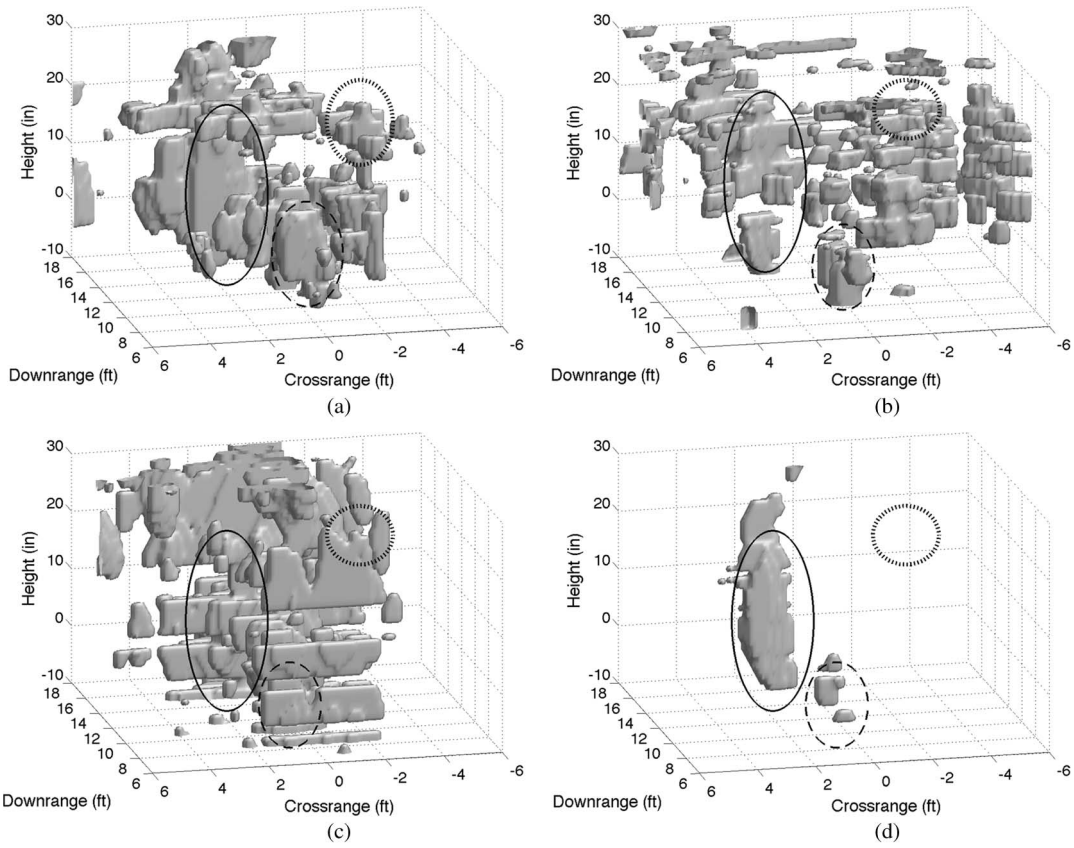

Fig. 8. Detection results of the iterative Bayes test of (solid) metal dihedral, (dotted) trihedral, and (dashed) sphere using single and full polarizations. Frequency weighting is used for wall removal. (a) 3-D detection HH. (b) 3-D detection VV. (c) 3-D detection HV. (d) 3-D detection full polarization.

shown in Fig. 7(d). It is clear that the dihedral and sphere are detected, whereas the trihedral goes unnoticed.

Similar results can be obtained by applying the iterative Bayes test as shown in Fig. 8. The targets in the single-polarization images are practically undetectable, whereas joint fusion and detection as per (5) enables detection of the sphere and dihedral.

IV. Experimental Results: Human

In addition to imaging of calibration metal targets, we consider the problem of detecting human behind walls. The problem of detecting a human behind walls or other visually opaque materials is of high importance in many TWRI applications, including hostage crisis, search and rescue missions, and military operations. When considering a human in motion, techniques such as Doppler analysis [17] and change detection [13], [25]–[27] can be used. The problem becomes more difficult when considering detection of stationary humans which may occur in resting, injury, or destressing situations.

The experimental setup is shown in Fig. 9, where the first author of this paper, C. Debes, is standing at approximately 12 ft down-range behind a concrete wall of thickness 5.625 in and dielectric constant 7.66. Imaging using a 2-D array, synthesized by a single antenna in motion as in Section III, is rather time consuming and requires the person to stand still for a relatively long time. Therefore, we employed a 1-D array

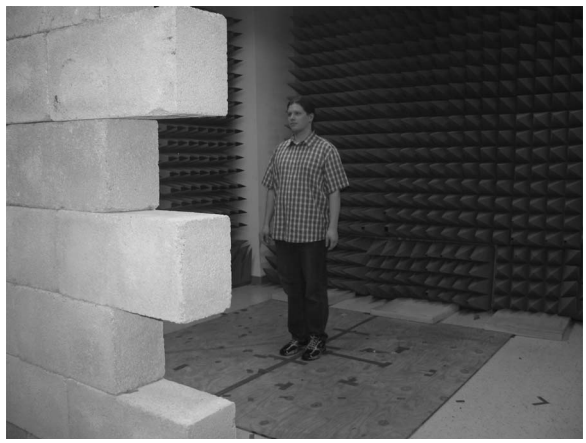

Fig. 9. Experimental setup: Human.

for this experiment. The array consists of 57 elements placed approximately 4 ft above the floor. The scene is imaged using VV, HH, and HV polarizations.

The resulting B-Scans using background subtraction as well as frequency weighting are shown in Fig. 10. The target reflection can be seen at approximately -1 ft cross-range and 11.5 ft down-range. Note that a human has a weak cross-polarization signature, which can be seen from Fig. 10(c) and (f). A target shadow can be observed approximately 1.5 ft behind the actual target position. This shadow stems from multipath propagation

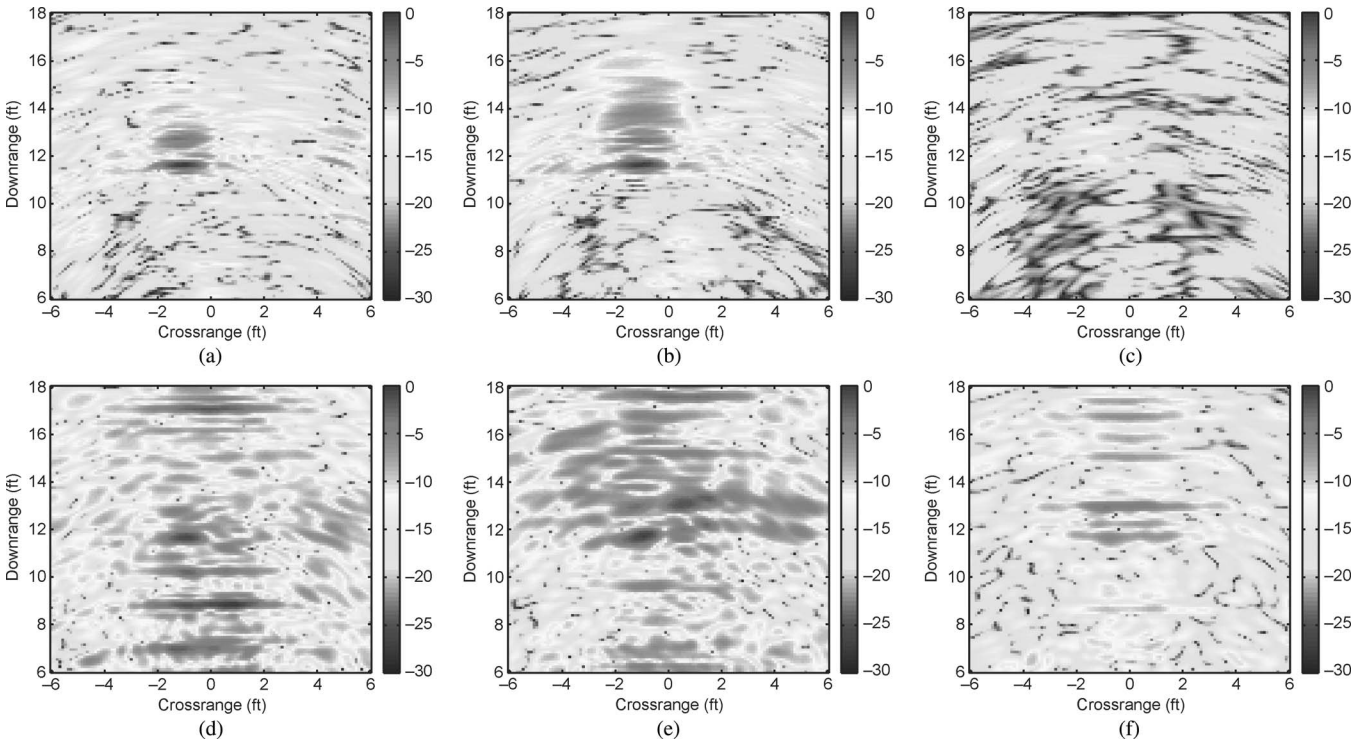

Fig. 10. Typical B-Scans of a human using different wall removal techniques. (a) Background subtraction, VV. (b) Background subtraction, HH. (c) Background subtraction, HV. (d) Frequency weighting, VV. (e) Frequency weighting, HH. (f) Frequency weighting, HV.

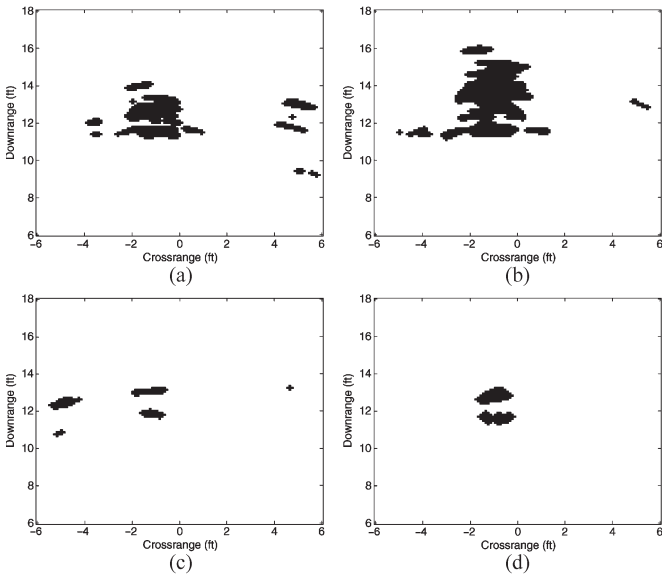

Fig. 11. Two-dimensional detection results of a human using the iterative NP test. Background subtraction is used for wall removal. (a) Human detection VV. (b) Human detection HH. (c) Human detection HV. (d) Human detection full polarization.

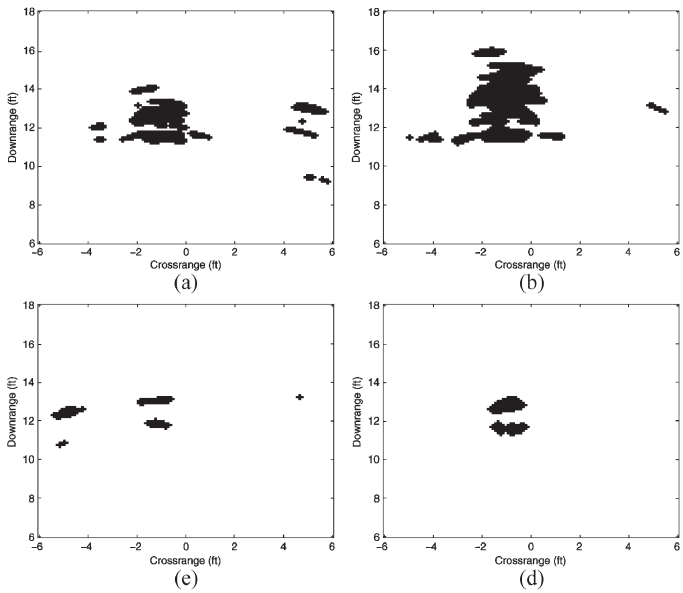

Fig. 12. Two-dimensional detection results of a human using the iterative Bayes test. Background subtraction is used for wall removal. (a) Human detection VV. (b) Human detection HH. (c) Human detection HV. (d) Human detection full polarization.

caused by the floor and appears strongly in the radar images as we only consider a 1-D array for imaging. Using a 2-D array would reduce this effect as the multipath propagation then differs with respect to the array height, whereas the target reflection always appears at the same position.

The 2-D detection results of the single as well as full polarized data can be seen in Figs. 11 and 12 for both detectors, as discussed in this paper. Here, background subtraction was used for wall removal, and a false-alarm rate of 5% was set for the iterative NP test, whereas a target pixel occupancy of 1% is fixed for the iterative Bayes test. We note that the target pixel occupancy, in practice, needs to be based on secondary information, i.e., the dimensions of the room, the average number

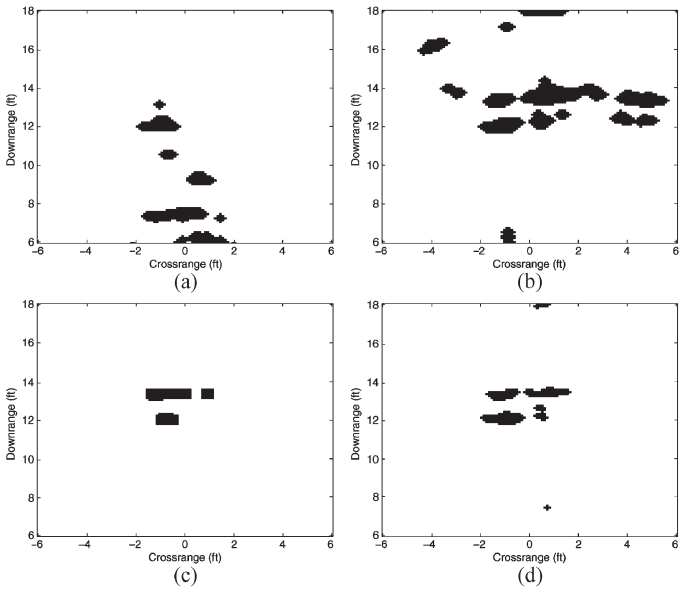

Fig. 13. Two-dimensional detection results of a human using the iterative NP test. Frequency weighting is used for wall removal. (a) Human detection VV. (b) Human detection HH. (c) Human detection HV. (d) Human detection full polarization.

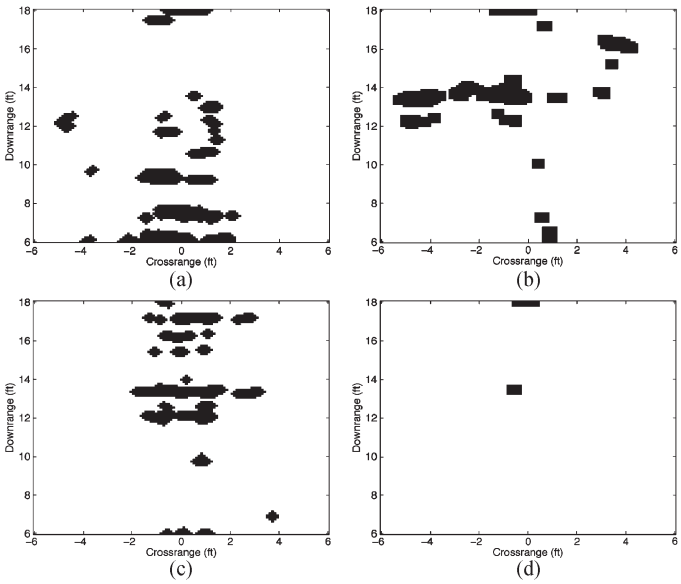

Fig. 14. Two-dimensional detection results of a human using the iterative Bayes test. Frequency weighting is used for wall removal. (a) Human detection VV. (b) Human detection HH. (c) Human detection HV. (d) Human detection full polarization.

of pixels, a human occupying for the specific imaging system, and the typical amount of targets in a room. This secondary information is highly application dependent.

It is clear that the individual detection results of VV, HH, and HV show clutter objects which render detection difficult. When joining all polarizations by the detectors introduced in Section II, an enhanced detection result as shown in Figs. 11(d) and 12(d) can be obtained. Here, clutter is completely removed, and we can clearly detect the human at approximately -1 ft cross-range and approximately 11.5 ft down-range. A similar performance for both introduced detectors is visible. The shadow target appearing due to multipath shows up approximately 1.5 ft behind the actual target. It is important to note that the shadow target is not considered as clutter or unwanted detection. It is a reflection which indirectly occurs due to the target presence at a position that can be estimated based on the target position. It is therefore a valuable information in performing target detection or follow-on tasks such as target classification.

The detection results when using the frequency weighting approach are shown in Figs. 13 and 14. Again, a general deterioration compared to the ideal scenario of using background subtraction can be observed. However, one can see that the usage of full polarization with the iterative detectors from Section II improves detection as shown in Figs. 13(d) and 14(d). The target and shadow reflections are separated, and few clutter objects appear due to the usage of a nonideal wall removal technique. We further observe a different performance for the iterative Bayes' test. Joint fusion and detection strongly suppresses the clutter but also reduces the probability of detection.

It is noted that the proposed detector has successfully been applied to a large number of TWRI scenarios with different objects and varying aspect angles. Due to space limitations, we restrict ourselves to the calibration setup in Fig. 3 and the human imaging setup in Fig. 9.

V. Conclusion

We have considered the problem of automatic target detection for targets behind walls using polarimetric imaging. A previously developed adaptive detection scheme has been extended to utilize the data from co- and cross-polarization arrays. Extensions include the ability to deal with image statistics which could vary with respect to antenna polarizations. In addition, an iterative version of Bayes' test is developed which allows adaptation to unknown and changing image statistics. When considering Bayes' test, a detection threshold is set that directly relates to image sparsity that is often encountered in TWRI. Given knowledge of the target voxel occupancy to be expected in a specific scenario, an optimal detector can be found. Experimental results using a calibration scene setup as well as of a human behind a wall have been conducted. The 2-D and 3-D detection results demonstrated the usefulness of the proposed detectors for TWRI applications. In all cases, a clear improvement in detection can be observed when jointly fusing the target information that is embedded in the co- and cross-polarization target returns. The proposed polarimetric detection approach assumes mitigation of wall clutter through the application of one of the effective techniques introduced in the literature. It is shown, however, that, in some cases, frequency weighting can reduce front wall sidelobes, unmasking targets and thus allowing detection to be performed.

References

[1] M. G. Amin, Ed., *Through-the-Wall Radar Imaging*. Boca Raton, FL: CRC Press, 2010.

[2] "Special issue on remote sensing of building interior," *IEEE Trans. Geosci. Remote Sens.*, vol. 47, no. 5, pp. 1267–1268, May 2009.

[3] E. Baranoski, "Through-wall imaging: Historical perspective and future directions," *J. Franklin Inst.*, vol. 345, no. 6, pp. 556–569, Sep. 2008.
[4] G. Alli and D. DiFilippo, "Beamforming for through-the-wall radar imaging," in *Through-the-Wall Radar Imaging*. Boca Raton, FL: CRC Press, 2010.
[5] F. Ahmad and M. G. Amin, "Multi-location wideband synthetic aperture imaging for urban sensing applications," *J. Franklin Inst.*, vol. 345, no. 6, pp. 618–639, Sep. 2008.
[6] C. Debes, M. G. Amin, and A. M. Zoubir, "Target detection in single- and multiple-view through-the-wall radar imaging," *IEEE Trans. Geosci. Remote Sens.*, vol. 47, no. 5, pp. 1349–1361, May 2009.
[7] C. Debes, J. Riedler, M. G. Amin, and A. M. Zoubir, "Iterative target detection approach for through-the-wall radar imaging," in *Proc. IEEE Int. Conf. Acoust. Speech Signal Process.*, 2009, pp. 3061–3064.
[8] C. Debes, J. Riedler, A. M. Zoubir, and M. G. Amin, "Adaptive target detection with application to through-the-wall radar imaging," *IEEE Trans. Signal Process.*, vol. 58, no. 11, pp. 5572–5583, Nov. 2010.
[9] B. G. Mobasseri and Z. Rosenbaum, "3-D classification of through-the-wall radar images using statistical object models," in *Proc. IEEE Workshop Image Anal. Interpretation*, 2008, pp. 149–152.
[10] B. G. Mobasseri, G. E. Smith, and I. Estephan, "A target alignment algorithm for through-the-wall radar imagery classification," in *Proc. IEEE Int. Radar Conf.*, 2010, pp. 756–761.
[11] C. Debes, J. Hahn, M. G. Amin, and A. M. Zoubir, "Feature extraction in through-the-wall radar imaging," in *Proc. IEEE Int. Conf. Acoust., Speech Signal Process.*, 2010, pp. 3562–3565.
[12] C. Debes, J. Hahn, A. M. Zoubir, and M. G. Amin, "Target discrimination and classification in through-the-wall radar imaging," *IEEE Trans. Signal Process.*, vol. 59, no. 10, pp. 4664–4676, Oct. 2011.
[13] A. R. Hunt, "Use of a frequency-hopping radar for imaging and motion detection through walls," *IEEE Trans. Geosci. Remote Sens.*, vol. 47, no. 5, pp. 1402–1408, May 2009.
[14] T. Dogaru and C. Le, "Through-the-wall small weapon detection based on polarimetric radar techniques," Army Res. Lab., Adelphi, MD, Tech. Rep., 2009.
[15] K. M. Yemelyanov, N. Engheta, A. Hoorfar, and J. A. McVay, "Adaptive polarization contrast techniques for through-wall microwave imaging applications," *IEEE Trans. Geosci. Remote Sens.*, vol. 47, no. 5, pp. 1362–1374, May 2009.
[16] M. Thiel and K. Sarabandi, "Ultra-wideband multi-static scattering analysis of human movement within buildings for the purpose of stand-off detection and localization," *IEEE Trans. Antennas Propag.*, vol. 59, no. 4, pp. 1261–1268, Apr. 2011.
[17] P. Setlur, F. Ahmad, M. G. Amin, and P. D. Zemany, "Experiments on through-the-wall motion detection and ranging," in *Proc. SPIE*, 2007, p. 653 809.
[18] Y.-S. Yoon and M. G. Amin, "Imaging of behind the wall targets using wideband beamforming with compressive sensing," in *Proc. IEEE Int. Workshop Stat. Signal Process.*, 2009, pp. 93–96.
[19] J.-S. Lee and E. Pottier, *Polarimetric Radar Imaging*. Boca Raton, FL: CRC Press, 2009.
[20] S. M. Kay, *Fundamentals of Statistical Signal Processing, Volume 2: Detection Theory*. Englewood Cliffs, NJ: Prentice-Hall, 1998.
[21] F. Ahmad and M. Amin, "Through-the-wall polarimetric imaging," in *Proc. SPIE*, 2008, pp. 69 700N-1–69 700N-10.
[22] J.-S. Lee, K. W. Hoppel, S. A. Mango, and A. R. Miller, "Intensity and phase statistics of multilook polarimetric and interferometric SAR imagery," *IEEE Trans. Geosci. Remote Sens.*, vol. 32, no. 5, pp. 1017–1028, Sep. 1994.
[23] R. Stevenson and G. Arce, "Morphological filters: Statistics and further syntactic properties," *IEEE Trans. Circuits Syst.*, vol. CAS-34, no. 11, pp. 1292–1305, Nov. 1987.
[24] A. V. Oppenheim and R. W. Schafer, *Discrete-Time Signal Processing*. Englewood Cliffs, NJ: Prentice-Hall, 2009.
[25] J. Moulton, S. Kassam, F. Ahmad, M. Amin, and K. Yemelyanov, "Target and change detection in synthetic aperture radar sensing of urban structures," in *Proc. IEEE Radar Conf.*, 2008, pp. 1–6.
[26] F. Soldovieri, R. Solimene, and R. Pierri, "A simple strategy to detect changes in through-the-wall imaging," *Progr. Electromagn. Res. M*, vol. 7, pp. 1–13, 2009.
[27] N. Maaref, P. Millot, P. Pichot, and O. Picon, "A study of UWB FM-CW radar for the detection of human beings in motion inside a building," *IEEE Trans. Geosci. Remote Sens.*, vol. 47, no. 5, pp. 1297–1300, May 2009.

Christian Debes (M'11) received the M.Sc. and Dr.-Ing. degrees in electrical engineering from Technische Universität Darmstadt, Darmstadt, Germany, in 2006 and 2010, respectively.

He worked as a Postdoctoral Research Fellow in the Signal Processing Group, Technische Universität Darmstadt. In 2011, he joined the R&D Center of AGT Germany as a Senior Researcher in the area of sensor networks for urban management and environmental sensing.

Abdelhak M. Zoubir (S'87–M'92–SM'97–F'08) received the Dr.-Ing. degree from Ruhr-Universität Bochum, Bochum, Germany, in 1992.

From 1992 to 1998, he was an Associate Professor with the Queensland University of Technology, Brisbane, Australia. In 1999, he joined the Curtin University of Technology, Perth, Australia, as a Professor of telecommunications and was Interim Head of the School of Electrical and Computer Engineering from 2001 to 2003. Since 2003, he has been a Professor and Head of the Signal Processing Group, Technische Universität Darmstadt, Darmstadt, Germany. His research interest lies in statistical methods for signal processing applied to telecommunications, sonar, radar, automotive safety and diagnosis, and biomedicine. He has published over 300 papers in these areas.

Dr. Zoubir was an Associate Editor of the IEEE TRANSACTIONS ON SIGNAL PROCESSING from 1999 to 2005 and has been a member of the Senior Editorial Board of the IEEE JOURNAL OF SELECTED TOPICS IN SIGNAL PROCESSING since 2009. He will begin his term as Editor-In-Chief of the IEEE SIGNAL PROCESSING MAGAZINE in January 2012. He is an IEEE Distinguished Lecturer (2010–2011). He is the Chair of the IEEE SPS Technical Committee Signal Processing Theory and Methods (he was its member from 2002 to 2007 and the Vice-Chair from 2008 to 2009). He has been a member of the IEEE SPS Technical Committee Sensor Array and Multi-Channel Signal Processing (SAM) since 2007 and was member of the IEEE SPS Technical Committee on Signal Processing Education (SpEd) from 2006 to 2008. He has been a member of the Board of Directors of the European Association for Signal Processing (EURASIP) since 2009 and is on the editorial board of the *EURASIP Journal on Advances in Signal Processing* and the *EURASIP Signal Processing Journal*. He was the Technical Chair of the 11th IEEE Workshop on Statistical Signal Processing (SSP 2001), held in Singapore in 2001; General Cochair of the 3rd IEEE International Symposium on Signal Processing and Information Technology (ISSPIT 2003), held in Darmstadt, Germany; General Cochair of the 5th IEEE Sensor Array and Multi-Channel Signal Processing Workshop (SAM 2008), held in Darmstadt in July 2008; and a member of the Technical Committee as Cochair for Plenary Sessions for ICASSP-08, held in Las Vegas, USA. He is the Technical Cochair of ICASSP-14 to be held in Florence, Italy. He has coauthored the papers that received the IEEE SPS Young Author Best Paper Award in 2003 and 2010.

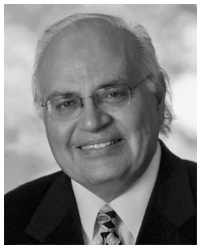

Moeness G. Amin (S'82–M'83–SM'91–F'01) received the Ph.D. degree in electrical engineering from the University of Colorado, Denver, in 1984.

He has been with the Faculty of the Department of Electrical and Computer Engineering, Villanova University, Villanova, PA, since 1985. In 2002, he became the Director of the Center for Advanced Communications, College of Engineering, Villanova University. He has over 450 journal and conference publications in the areas of wireless communications, time–frequency analysis, smart antennas, waveform design and diversity, interference cancellation in broadband communication platforms, anti-jam GPS, target localization and tracking, direction finding, channel diversity and equalization, ultrasound imaging, and radar signal processing.

Dr. Amin currently serves on the overview board of the IEEE TRANSACTIONS ON SIGNAL PROCESSING. He also serves on the editorial board of the *EURASIP Signal Processing Journal*. He was a member of the IEEE Signal Processing Society Technical Committee on Statistical Signal and Array Processing from 1995 to 1997. He was also a member of the IEEE Signal Processing Society Technical Committee on Signal Processing for Communications from 1998 to 2002. He was a Distinguished Lecturer of the IEEE Signal Processing Society from 2003 to 2004. He is a Fellow of the International Society of Optical Engineering and a Fellow of the Institute of Engineering and Technology. He is an active member of the Franklin Institute Committee on Science and the Arts. He was the General and Organization Chair of the IEEE International Symposium on Time-Frequency and Time-Scale Analysis in 1994. He was an Associate Editor of the IEEE TRANSACTIONS ON SIGNAL PROCESSING from 1996 to 1998. He was the General and Organization Chair of the IEEE Workshop on Statistical Signal and Array Processing in 2000. He was the Technical Program Chair of the 2nd IEEE International Symposium on Signal Processing and Information Technology in 2002. He was the Special Session Cochair of the 2008 IEEE International Conference on Acoustics, Speech, and Signal Processing. He was a Plenary Speaker at ICASSP 2010. He has given several keynote and plenary talks and served as a Session Chair in several technical meetings. He organized seven workshops and seminars for the Franklin Institute Medal Program and the IEEE Philadelphia Section. He was the Guest Editor of the *Journal of the Franklin Institute* (September 2008) Special Issue on Advances in Indoor Radar Imaging; the IEEE TRANSACTIONS ON GEOSCIENCE AND REMOTE SENSING May-09 Special Issue on Remote Sensing of Building Interior; and the *IET Signal Processing* (December 2009) Special Issue on Time-Frequency Approach to Radar Detection, Imaging, and Classification. He is the Editor of the first book *Through-the-Wall Radar Imaging* (CRC Press). He was a recipient of seven best paper awards. He was also a recipient of the Villanova University Outstanding Faculty Research Award in 1997, the IEEE Philadelphia Section Award in 1997, the IEEE Third Millennium Medal in 2000, and the Chief of Naval Research Challenge Award in 2010. He was also a recipient of the 2009 Individual Technical Achievement Award from the European Association of Signal Processing and the 2010 NATO Scientific Achievement Award. He is a member of SPIE, EURASIP, ION, Eta Kappa Nu, Sigma Xi, and Phi Kappa Phi.